Electron scattering by methane: Elastic scattering and rotational excitation cross sections calculated with ab initio interaction potentials

Najib Abusalbi, Robert A. Eades, Tonny Nam, Devarajan Thirumalai, David A. Dixon et al.

Citation: J. Chem. Phys. **78**, 1213 (1983); doi: 10.1063/1.444914
View online: http://dx.doi.org/10.1063/1.444914
View Table of Contents: http://jcp.aip.org/resource/1/JCPSA6/v78/i3
Published by the American Institute of Physics.

Electron scattering by methane: Elastic scattering and rotational excitation cross sections calculated with *ab initio* interaction potentials

Najib Abusalbi, Robert A. Eades, Tonny Nam,[a] Devarajan Thirumalai,[b] David A. Dixon, and Donald G. Truhlar

Department of Chemistry and Chemical Physics Program, University of Minnesota, Minneapolis, Minnesota 55455

Michel Dupuis[c]

National Resource for Computation in Chemistry, Lawrence Berkeley Laboratory, Berkeley, California 94720
(Received 24 May 1982; accepted 18 June 1982)

We calculate *ab initio* interaction potentials for electron-methane scattering and use them to perform converged scattering calculations for the electronically and vibrationally elastic rotational-state-to-rotational-state cross sections at 10 eV impact energy. The effective potential has static, local exchange, and polarization terms calculated from extended-basis-set Hartree–Fock wave functions for both unperturbed and polarized methane molecules. The polarization potential includes nonadiabatic effects in the semiclassical local kinetic energy approximation, and for comparison we also perform calculations based on the adiabatic polarization potentials. Five to 12 terms are retained in the angular expansion of the various parts of the interaction potential and the coupled channels calculations involved 41 total angular momenta, with 1–33 coupled channels for each. The resulting rotationally summed integral cross sections are in excellent agreement with recent experiments for scattering angles 40° and larger, but are larger than the experiment at small scattering angles. The rotationally inelastic cross sections for the full potential are smaller than those for the adiabatic potential by about a factor of 2.

I. INTRODUCTION

Most quantum mechanical calculations of electron-molecule scattering have been for linear molecules. In that case there are important simplifications in the calculation of the target wave function and effective interaction potential and in the solution of the scattering equations.[1] Burke *et al.*[2] have developed a formalism for treating electron scattering by general polyatomic molecules in the fixed-nuclei approximation. The scattering amplitudes of this method may be used to calculate state-to-state cross sections in the vibrational-rotational sudden approximation, which is expected to be a good approximation for nondipole cases except near thresholds. In this article we present a laboratory-frame calculation for electron scattering by a nonlinear molecule, namely methane. This has the advantage of yielding state-to-state cross sections directly. We make the rigid-rotator approximation and calculate differential and integral cross sections for pure elastic scattering and for state-to-state rotational excitation processes. We use a general formalism that takes full advantage of the T_d symmetry of the rigid methane molecule. The calculations are carried out for an impact energy of 10 eV. This energy is at the border of the low- and intermediate-energy regions; as far as computational difficulty this energy involves a compromise between the simplification of the rapid convergence of the sum over orbital angular momentum contributions at low energy and the greater validity at intermediate and high energy of local approximations[3] for the electron-target exchange interactions. The border of low- and intermediate-energy is also a crucial one for testing approximations in the treatment of charge polarization (see the next paragraph), and it allows for comparison to the experimental differential cross section measurements of Rohr,[4] Tanaka and co-workers,[5] and Newell *et al.*[6] and to the model potential calculations performed by Gianturco and Thompson[7,8] using a simple model potential and the formalism of Burke *et al.*[2,9]

Although it has been demonstrated in previous work that nonempirical scattering calculations based on neglect of differential overlap molecular orbital theory, local exchange approximations, and minimum-basis-set polarization potentials can yield useful accuracy for e^--N_2, e^--CO, e^--C_2H_2, and e^--CO_2 scattering at 10 eV and above,[10] it is also of interest to explore more *ab initio* treatments. In the present paper we again use local exchange approximations, but we calculate the static potential and the target density for the exchange potential by extended-basis-set Hartree–Fock calculations. Furthermore, we approximate the effect of charge polarization in two different ways: by an *ab initio* extended basis set adiabatic polarization potential V^{Pa} and also by the local-kinetic energy semiclassical polarization potential V^{Plke}. The latter is an approximation[11] to the true polarization potential, defined as the difference between the real part of the exact optical potential and the static-exchange potential. V^{Plke} is computationally convenient because it can be calculated from the *ab initio* static and adiabatic polarization potentials, and hence it provides a way to modify V^{Pa} to account for nonadiabatic effects.

II. SCATTERING THEORY

In this section we present a laboratory-frame formalism for scattering of a structureless particle by a spherical top molecule with T_d symmetry. It is very

[a] Lando Summer Undergraduate Research Fellow, 1981.
[b] Present address: Department of Chemistry, Columbia, University, New York, NY 10027.
[c] Present address: Materials and Molecular Research Division, Lawrence Berkeley Laboratory, Berkeley, CA 94720.

 0021-9606/83/031213-15$2.10

similar to the formalism used by Secrest and coworkers[12] for Ar–CH_4 scattering; however their formalism only took advantage of the T subgroup of T_d. Furthermore, we present our formalism in a general way so that it is reasonably clear how to modify it to treat the scattering of structureless particles by other nonlinear molecules having different symmetry point groups.

The total wave function of definite total angular momentum J and projection M on the laboratory z axis is expressed as

$$\Psi^{JM}(\mathbf{r},\mathrm{G})=\sum_{j=0}^{\infty}\sum_{\alpha=1}^{\alpha_{\max}(j)}\sum_{l=|J-j|}^{J+j} r^{-1} f^{J}_{j\alpha l}(r)\mathcal{Y}^{JM}_{j\alpha l}(\hat{r},\mathrm{G}) \ . \tag{1}$$

In practice, the close coupling approximation cuts off the sum over j at some finite $j_{\max}$ which is a decreasing function of J. The vector G specifies the orientation (α,β,γ) of the molecule with respect to the laboratory-frame axes, r is the distance from the center of mass of the rotor to the scattering electron, and $\hat{r}$ specifies the angular position (θ,ϕ) of the incident electron, again with respect to laboratory-frame axes. The expansion coefficients $f^{J}_{j\alpha l}(r)$ are the scattering-particle radial wave functions. The total angular momentum eigenfunction $\mathcal{Y}^{JM}_{j\alpha l}$, where j is the rotational quantum number, α specifies a particular member of the degenerate set for a given j, and l specifies the orbital angular momentum of the scattering particle, is defined in terms of rotor and projectile angular functions as

$$\mathcal{Y}^{JM}_{j\alpha l}(\hat{r},\mathrm{G})=\sum_{m_l=-l}^{l}\sum_{m_j=-j}^{j}(lm_l jm_j|ljJM)\psi_{j\alpha m_j}(\alpha,\beta,\gamma)Y^{m_l}_{l}(\theta,\phi), \tag{2}$$

where $(lm_l jm_j|ljJM)$ is a Clebsch–Gordan coefficient. (All angular momentum coupling coefficients are defined as in Edmonds.[13]) $\psi_{j\alpha m_j}(\alpha,\beta,\gamma)$ is a rotor wave function. The rotor wave functions for spherical tops are the rotation matrices[13] $\mathfrak{D}^{(j)}_{km_j}(\alpha,\beta,\gamma)$ for the finite rotations specified by the Euler angles α, β, and γ, which are collectively denoted as G. In the rotor function m_j is the projection of j on the laboratory z axis, and k is its projection on the rotor z axis. The spherical top rotor states have a degeneracy of $(2j+1)^2$, i.e.,

$$H_{\mathrm{rotor}}(\alpha,\beta,\gamma)\mathfrak{D}^{(j)}_{km_j}(\alpha,\beta,\gamma)=Bj(j+1)\mathfrak{D}^{(j)}_{km_j}(\alpha,\beta,\gamma) \tag{3}$$

for $-j\le k\le j$ and $-j\le m_j\le j$, where B is the rotational constant; thus we may take any convenient linear combinations as our basis functions. We choose linear combinations that transform as the irreducible representations of the T point group, i.e.,

$$\psi^{p\mu}_{jhm_j}(\alpha,\beta,\gamma)=A^{p\mu}_{jhm_j}\sum_{k=-j}^{j}\langle jk|jp\mu h\rangle\mathfrak{D}^{(j)}_{km_j}(\alpha,\beta,\gamma) \ , \tag{4}$$

where $A^{p\mu}_{jhm_j}$ is a normalization constant, p specifies the symmetry (A, E, or T), μ specifies the component of the representation ($\mu=1$ for A, 1 or 2 for E, and 1, 2, or 3 for T), and h specifies the hth basis function of rotational quantum number j for a given p and μ. Now the sum over α in Eq. (1) becomes a sum over p, μ, and h.

We will require the matrix elements of the interaction potential between total angular momentum eigenfunctions

$$V^{J}_{j\alpha lj'\alpha' l'}(r)=\int d\hat{r}\int d\mathrm{G}\,\mathcal{Y}^{JM*}_{j\alpha l}(\hat{r},\mathrm{G})\times V(\mathbf{r},\mathrm{G})\mathcal{Y}^{JM}_{j'\alpha' l'}(\hat{r},\mathrm{G}) \ . \tag{5}$$

The interaction potential transforms according to the group T_d and may be written as

$$V(\mathbf{r},\mathrm{G})=\sum_{\lambda=0}^{\infty}\sum_{i=1}^{i_{\max}(\lambda)}V_{\lambda i}(r)T_{\lambda i}(\theta,\phi,\alpha,\beta,\gamma) \ , \tag{6}$$

where $i_{\max}(\lambda)$ is the number of A_1 basis functions with λ nodes in the θ variable, and

$$T_{\lambda i}(\theta,\phi,\alpha,\beta,\gamma)=\zeta_\lambda\sum_{s=-\lambda}^{\lambda}\sum_{q=-\lambda}^{\lambda}a^{\lambda}_{iq}\,\mathfrak{D}^{(\lambda)*}_{qs}(\alpha,\beta,\gamma)Y^{s}_{\lambda}(\theta,\phi) \ , \tag{7}$$

where ζ_λ is a phase factor chosen as

$$\zeta_\lambda=\begin{cases}+1 \ , & \text{even } \lambda \ ,\\ -i \ , & \text{odd } \lambda \ ,\end{cases} \tag{8}$$

so that $V_{\lambda i}(r)$ is always real, and a^{λ}_{iq} is a real coefficient chosen so that $T_{\lambda i}(\theta,\phi,\alpha,\beta,\gamma)$ transforms under the symmetry operators of the T_d point group according to the A_1 irreducible representation; in particular, $\zeta_\lambda a^{\lambda}_{iq}=\langle\lambda q|\lambda A_1 1i\rangle$. Thus, for any θ, ϕ, if $\hat{S}$ reorients the rotor (i.e., G) according to a rotation of T_d, then

$$\hat{S}T_{\lambda i}(\theta,\phi,\alpha,\beta,\gamma)=(+1)T_{\lambda i}(\theta,\phi,\alpha,\beta,\gamma) \ . \tag{9}$$

Of course one can also hold the rotor fixed at $\alpha=\beta=\gamma=0$, for which $\mathfrak{D}^{(\lambda)}_{qs}(0,0,0)=\delta_{sq}$, and reorient the scattering particle (i.e., θ, ϕ). Equation (9) holds for this kind of symmetry operation too, and also for the improper rotations of T_d. The latter interpretation provides a more convenient method for deriving the coefficients a^{λ}_{iq}, and they have been derived by Altmann and Cracknell[14] in this way. Their choice of axes corresponds to reflections in the xy, xz, and yz planes all being symmetry operators; to be consistent with this we let $\alpha=\beta=\gamma=0$ correspond to $x_{\mathrm{H}}=y_{\mathrm{H}}=z_{\mathrm{H}}<0$ when x_{H}, y_{H}, and z_{H} are the Cartesian coordinate of one of the hydrogen atoms. For this choice the required coefficients can be obtained from the following expression:

$$a^{l}_{g,\pm m}=\begin{cases}\bar{a}^{l}_{m} & , \ m=0 \ ,\\ (\mp i)^{\nu}\ \bar{a}^{l}_{m}/\sqrt{2} & , \ m\neq 0 \ ,\end{cases} \tag{10}$$

where $\bar{a}^{l}_{m}$ is the quantity tabulated by Altmann and Cracknell for the gth component for a given l of the A_1 representation, and ν is 0 or 1 for functions containing $\cos m\phi$ or $\sin m\phi$. Note there is a sign error in $\bar{a}^{11}_{2}$ in their Table I; the correct value is $-0.665\,363\,31$.

Substituting Eqs. (2), (4), (6), and (7) into Eq. (5) yields

$$V^{J}_{j\alpha lj'\alpha' l'}(r)=\sum_{m_l}\sum_{m_j}\sum_{m_{l'}}\sum_{m_{j'}}\sum_{\lambda}\sum_{i}\sum_{s}(lm_l jm_j|ljJM)(l'm_{l'},j'm_{j'}|l'j'JM)V_{\lambda i}(r)\zeta_\lambda \times\int d\hat{r}\,Y^{m_l*}_{l}(\hat{r})\,Y^{s}_{\lambda}(\hat{r})\,Y^{m_{l'}}_{l'}(\hat{r})\int d\mathrm{G}\,\psi^{p\mu*}_{jhm_j}(\mathrm{G})\Big[\sum_{q=-\lambda}^{\lambda}a^{\lambda}_{iq}\,\mathfrak{D}^{(\lambda)*}_{qs}(\mathrm{G})\Big]\psi^{p'\mu'}_{j'h'm_{j'}}(\mathrm{G}) \ . \tag{11}$$

TABLE I. Decomposition of the rotational basis in T_d symmetry.

λ	Number of terms in potential (with A_1 symmetry)	j	Number of A_1 rotational basis functions	Number of channel functions with symmetry A_1 and index $(-1)^J$
0	1	0	1	1
1, 2	0	1, 2	0	0
3, 4	1	3, 4	$2j+1$	$j+1$
5	0	5	0	0
6–11	1	6–11	$2j+1$	$j+1$
12	2	12	50	26
13, 14	1	13, 14	$2j+1$	$j+1$

According to the discussion above [first interpretation of $\hat{S}$ in Eq. (9)], the quantity in brackets has A symmetry; therefore[15] the integral over **G** is proportional to $\delta_{pp'}\delta_{\mu\mu'}$. Thus, the problem is block diagonal in p and μ. Furthermore, if the $\langle jk|jp\mu h\rangle$ coefficients of Eq. (4) and hence the rotor states are formally classified as A_1 or A_2 according to the scheme of Altmann and Cracknell,[14] one finds that matrix elements coupling the $J=0$ rotor state to A_2 rotor states vanish.

We restrict our attention in the rest of this paper to the case where the rotor is initially in the ground rotational state. This state is nondegenerate with A_1 symmetry, and we restrict our basis set to rotor functions with A_1 symmetry. For convenience, for A_1 basis functions, we rewrite Eq. (4) in the normalized form

$$\psi_{jk m_j}(\alpha,\beta,\gamma)=N_j \exp[ik_{\max}(j,h)\pi/4]\sum_{k=-k_{\max}(j,h)}^{k_{\max}(j,h)} a_{hk}^{j}\,\mathfrak{D}_{km_j}^{(j)}(\alpha,\beta,\gamma)\ , \tag{12}$$

where

$$N_j=[(2j+1)/8\pi^2]^{1/2}\ , \tag{13}$$

and where $k_{\max}(j,h)$ is the highest value of k for which a_{hk}^{j} is nonzero. Using basis function (12), the matrix element (11) becomes

$$V^J_{jhlj'h'l'}(r)=N_jN_{j'}\exp[i(k'_{\max}-k_{\max})\pi/4]\sum_{m_l}\sum_{m_j}\sum_{m_{l'}}\sum_{m_{j'}}\sum_{l}\sum_{i}\sum_{s}\sum_{k}\sum_{k'}\sum_{q}\zeta_\lambda a^{\lambda}_{lq}a^{j}_{hk}a^{j'}_{h'k'}V_{\lambda i}(r)$$
$$\times(lm_l jm_j|ljJM)(l'm_{l'}j'm_{j'}|l'j'JM)\int d\hat{r}\,Y_l^{m_l*}(\hat{r})Y_\lambda^{s}(\hat{r})Y_{l'}^{m_{l'}*}(\hat{r})\int d\mathbf{G}\,\mathfrak{D}^{(j)*}_{km_j}(\mathbf{G})\mathfrak{D}^{(\lambda)*}_{qs}(\mathbf{G})\mathfrak{D}^{(j')}_{k'm_{j'}}(\mathbf{G})\ . \tag{14}$$

The integral over $\hat{r}$ can be done in terms of $3j$ symbols using Eqs. (2.5.6) and (4.6.3) of Edmonds,[13] and the integral over G can be done in terms of $3j$ symbols using his Eqs. (4.2.7) and (4.6.2). This yields

$$V^J_{jhlj'h'l'}(r)=N_j\text{ ---}\sum_q 8\pi^2[(2l+1)(2l'+1)(2\lambda+1)/4\pi]^{1/2}\zeta_\lambda V_{\lambda i}(r)a^{\lambda}_{lq}a^{j}_{hk}a^{j'}_{h'k'}(lm_l jm_j|ljJM)(l'm_{l'}j'm_{j'}|l'j'JM)$$
$$\times(-1)^{m_l+m_j-s-k-q}\begin{pmatrix} l & \lambda & l' \\ 0 & 0 & 0\end{pmatrix}\begin{pmatrix} l & \lambda & l' \\ -m_l & s & m_{l'}\end{pmatrix}\begin{pmatrix} j & \lambda & j' \\ -m_j & -s & m_{j'}\end{pmatrix}\begin{pmatrix} j & \lambda & j' \\ -k & -q & k'\end{pmatrix}\ , \tag{15}$$

where the --- denotes that the beginning of the right-hand side is the same as in the previous equation. This expansion may be further simplified by introducing a $6j$ symbol as defined in Eq. (6.2.3) of Edmonds, i.e.,

$$V^J_{jhlj'h'l'}(r)=(-1)^{J+l+l'}8\pi^2N_jN_{j'}\exp[i(k'_{\max}-k_{\max})\pi/4][(2l+1)(2l'+1)/4\pi]^{1/2}\sum_\lambda\zeta_\lambda(2\lambda+1)^{1/2}$$
$$\times\begin{pmatrix} l & \lambda & l' \\ 0 & 0 & 0\end{pmatrix}\begin{Bmatrix} j & l & J \\ l' & j' & \lambda\end{Bmatrix}\sum_i V_{\lambda i}(r)\sum_k(-1)^{-k}a^{j}_{hk}\sum_{k'}a^{j'}_{h'k'}\sum_q(-1)^{-q}a^{\lambda}_{lq}\begin{pmatrix} j & \lambda & j' \\ -k & -q & k'\end{pmatrix}\ . \tag{16}$$

This expression simplifies for $\lambda=0$, hence it can be rewritten in the following convenient form:

$$V^J_{jhlj'h'l'}(r)=\delta_{jj'}\delta_{hh'}\delta_{ll'}(4\pi)^{-1/2}V_{01}(r)+\sum_{\lambda>0}\sum_i B^J_{jhlj'h'l';\lambda i}V_{\lambda i}(r)\ , \tag{17}$$

where

$$B^J_{jhlj'h'l';\lambda i}=(-1)^{J+\lambda}\exp[i(k'_{\max}-k_{\max})\pi/4][(2l+1)(2l'+1)(2\lambda+1)(2j+1)(2j'+1)/4\pi]^{1/2}\zeta_\lambda$$
$$\times\begin{pmatrix} l & l' & \lambda \\ 0 & 0 & 0\end{pmatrix}\begin{Bmatrix} j & l & J \\ l' & j' & \lambda\end{Bmatrix}\sum_k(-1)^{-k}a^{j}_{hk}\sum_{k'}a^{j'}_{h'k'}\sum_q(-1)^{-q}a^{\lambda}_{lq}\begin{pmatrix} j & \lambda & j' \\ -k & -q & k'\end{pmatrix}\ , \tag{18}$$

in which we replaced N_j and $N_{j'}$ by their corresponding expressions and permuted the $3j$ symbol $\begin{pmatrix} l & \lambda & l' \\ 0 & 0 & 0 \end{pmatrix}$ to $\begin{pmatrix} l & l' & \lambda \\ 0 & 0 & 0 \end{pmatrix}$. The selection rules associated with the $3j$ symbols in Eq. (18) restrict the number of nonzero matrix elements as follows:

$$\max(|j'-j|, |l'-l|) \leq \lambda \leq \min(j'+j, l'+l) , \tag{19}$$

$$l + l' + \lambda = \text{even} , \tag{20}$$

and

$$k' - k - q = 0 . \tag{21}$$

The potential matrix is symmetric and real. Its reality is ensured by the proper phase factor chosen above, namely $\zeta_\lambda \exp[i(k'_{\max} - k_{\max})\pi/4]$. Notice that according to the conventions adopted here the spherical average of the potential becomes $V_{01}(r)/(4\pi)^{1/2}$, not $V_{01}(r)$.

Substituting Eqs. (1)–(3) and (12) into the complete Schrödinger equation and requiring

$$\int d\hat{r} \int d\mathbf{G}\, \mathcal{Y}^{JM*}_{j'k'l'}(\hat{r}, \mathbf{G})(H - E)\Psi^{JM}(\mathbf{r}, \mathbf{G}) = 0 \tag{23}$$

yields the close coupling equations

$$\left[-\frac{\hbar^2}{2m}\frac{d^2}{dr^2} + V^J_{jhljhl}(r) - \frac{\hbar^2 k_j^2}{2m}\right] f^J_{jhl}(r)$$
$$= \sum_{j'k'l'} V^J_{jhlj'k'l'}(r) f^J_{j'k'l'}(r) , \tag{24}$$

where

$$k_j^2 = (2m/\hbar^2)[E - Bj(j+1)] \tag{25}$$

and E is the total energy. These equations are to be solved subject to the usual scattering boundary conditions to yield the transition matrix elements $T^J_{jhlj'k'l'}$. From these the differential and integral cross sections $d\sigma_{jj'}/d\Omega$ and $\sigma_{jj'}$ may be calculated by the formulas of Blatt and Biedenharn[16,17] and the momentum transfer cross sections may be calculated by

$$\sigma^m_{jj'} = 2\pi \int_0^\pi d\theta \sin\theta(1 - \cos\theta) d\sigma_{jj'}/d\Omega . \tag{26}$$

To the extent that the interaction potential for the rigid rotator approximates that for the vibrationally averaged rotor the electronically and vibrationally elastic total cross sections may be obtained by summing over j' for $j = 0$. The resulting cross sections will be called the vibrationally elastic cross sections and labeled $d\sigma_0/d\Omega$, σ_0, and σ^m_0.

The restriction to A_1 symmetry states greatly reduces the number of channels that couple to the ground state. The number of channels that must be considered is further reduced by parity-like considerations. The parity-like index of a channel defined by Eqs. (2) and (12) is defined as $(-1)^{j+l}$. The index of the ground-state channel is thus $(-1)^J$. Channels with different signs of the index are uncoupled. The resulting savings are summarized in Table I. For typical low-j values the number of channels that must be considered is $(j+1)$, as compared to the degeneracy of $(2j+1)^2$ for a given j if neither symmetry nor the index is considered. The last column of Table I is actually the maximum number of channels that must be considered and applies in the large-J limit. At low J the number of channel functions is further restricted by the triangle inequality

$$|J - j| \leq l \leq J + j . \tag{27}$$

We would like to emphasize the enormous savings that are achieved by considering both symmetry and the parity-like index as compared to the case when only the latter is considered. For example, for $J = 3$, the number of channels for $j_{\max} = 11$ is reduced from 562 when only the index is considered to 33 when the full symmetry of CH_4 is considered. This reduction in the number of channels corresponds to a savings of a factor of about 5×10^3 in computer time.

III. CALCULATION OF THE INTERACTION POTENTIAL

For all calculations the C–H bond distance is fixed at $2.0441 a_0$, which is the optimum value at the Hartree–Fock level for the basis set of Scanlon *et al.*[18]

The present calculations were performed using an extended basis set including polarization functions and diffuse functions. This basis set was chosen by analogy to the nitrogen[19(a)] and water[19(b)] molecules, for which we had previously made extensive comparisons of polarization potentials and polarizabilities calculated with various basis sets. The basis chosen for CH_4 is denoted (12, 8, 3/8, 3)/[9, 7, 3/7, 3] in the usual notation. This basis was obtained by starting with the Huzinaga (11, 7) carbon basis[20(a)] and contracting the first four s functions with the atomic $1s$ coefficients and the first two p functions with the $2p$ coefficients. Diffuse s and p functions were added by geometric expansion. Valence $3d$ polarization functions were added with exponential parameters (1.5, 0.35) taken from van Duijneveldt,[20(b)] and another polarization function was added with an exponential parameter (0.08) optimized for the polarizability of methane by Werner and Meyer.[21] For hydrogen we used Huzinaga's[22] seven s functions with the first two contracted plus a diffuse s function obtained by geometric expansion. Three p functions with exponential parameters 1.8, 0.6, and 0.2 were also added. The value 0.2 is taken from Werner and Meyer[21] and the other functions have parameters differing by factors of 3 and 9. Putting these functions together yields 122 primitives and 112 contracted functions, which are combined into canonical orthonormal orbitals. To avoid linear dependency, only 111 of the canonical orthonormal orbitals are kept for the final calculations.

The wave functions, all the polarization potentials, and many of the static potentials were calculated on a CDC 7600 computer using the program MDHONDO.[23] The rest of the static potentials were calculated on a VAX 11/780 computer using a modified version of the NYU Gaussian properties program.[24]

The static and adiabatic polarized potentials $V^S(\mathbf{r}, \mathbf{G})$ and $V^{SPa}(\mathbf{r}, \mathbf{G})$ are defined elsewhere.[25] In particular they represent the interaction of a negative test charge with the unperturbed and fully relaxed target charge clouds, respectively.

The adiabatic polarization potential is then defined by

$$V^{Pa}(\mathbf{r}, \mathbf{G}) = V^{SPa}(\mathbf{r}, \mathbf{G}) - V^S(\mathbf{r}, \mathbf{G}) . \tag{28}$$

The energy-dependent exchange potential $V^{E}(\mathbf{r}, \mathbf{G}, E)$ was calculated from the static target density by the semiclassical exchange approximation[3]

$$V^{E}(\mathbf{r}, \mathbf{G}, E) = \tfrac{1}{2}[E - V^{S}(\mathbf{r}, \mathbf{G})] - \tfrac{1}{2}\{[E - V^{S}(\mathbf{r}, \mathbf{G})]^2 + 4\pi\rho(\mathbf{r}, \mathbf{G})\}^{1/2} , \quad (29)$$

where $\rho(\mathbf{r}, \mathbf{G})$ is the electronic charge density of the unperturbed target.

The adiabatic model overestimates the polarization effect, even at low impact energies, because the scattering electron is speeded up by the field of the target and the target polarization does not have enough time to respond fully to the scattered charge. We attempt to account for this effect by the local kinetic energy semiclassical polarization model presented elsewhere.[11] In this model the polarization potential is

$$V^{\mathrm{Plke}}(\mathbf{r}, \mathbf{G}, E) = [1 + T_{\mathrm{loc}}(\mathbf{r}, \mathbf{G}, E)/\Delta]^{-1} V^{\mathrm{Pa}}(\mathbf{r}, \mathbf{G}) , \quad (30)$$

where Δ is the effective excitation energy, $T_{\mathrm{loc}}(\mathbf{r}, \mathbf{G}, E)$ is the local kinetic energy

$$T_{\mathrm{loc}}(\mathbf{r}, \mathbf{G}, E) = E - V^{SE}(\mathbf{r}, \mathbf{G}, E) , \quad (31)$$

and $V^{SE}(\mathbf{r}, \mathbf{G}, E)$ is the static-exchange potential

$$V^{SE}(\mathbf{r}, \mathbf{G}, E) = V^{S}(\mathbf{r}, \mathbf{G}) + V^{E}(\mathbf{r}, \mathbf{G}, E) . \quad (32)$$

The total potential used in the scattering calculations is the sum of $V^{SE}(\mathbf{r}, \mathbf{G}, E)$ and either $V^{\mathrm{Pa}}(\mathbf{r}, \mathbf{G})$ or $V^{\mathrm{Plke}}(\mathbf{r}, \mathbf{G}, E)$.

The effective excitation energy is most readily evaluated by the method used by Slater and Kirkwood[26] for approximating the dispersion interaction between two atoms or molecules. This yields[27,28]

$$\Delta = (N_{\mathrm{val}}/\alpha_d)^{1/2} , \quad (33)$$

where N_{val} is the number of electrons in the outer shell of the molecule and α_d is the static dipole polarizability. Using $N_{\mathrm{val}} = 8$ and the most accurate available value[28] for α_d yields $\Delta = 18.52$ eV, which is somewhat higher than the ionization potential (12.98 eV).[29]

The actual orientation $(\mathbf{r}, \mathbf{G})$ at which the potentials were calculated are most conveniently specified in relative coordinates (χ, ϕ_χ). These are values of (θ, ϕ) when G is chosen to put one C–H bond on the positive z axis. Then the region to be covered by actual calculations is $0 \le \chi \le 4\tau$ and $0 \le \phi_\chi \le 60°$. Here τ is one eighth the HCH bond angle and equals 13.68°. Values of χ and ϕ_χ outside the region all correspond by symmetry to a value within the region. The static and exchange potentials were calculated for 12 different orientations $(\chi, \phi_\chi) = (0, 0)$, $(2\tau, 0)$, $(2\tau, 60)$, $(4\tau, 0)$, $(4\tau, 60)$, $(0.5\tau, 30)$, $(\tau, 30)$, $(2\tau, 30)$, $(3\tau, 0)$, $(3\tau, 30)$, $(3\tau, 60)$, and $(4\tau, 30)$ for each of 26 values of r in the range 0.1–$6.4a_0$ and for the first five of these orientations for each of three values of r in the range 10–$30a_0$. Additional calculations at $(\tau, 0)$ and $(\tau, 60)$ were carried out for $r = 1.0$–$3.1a_0$. The adiabatic polarization potential was calculated for the first five orientations for each of 19 values of r in the range 0.1–$30a_0$. These values are used to generate a combined analytic and spline representation of the full potentials (SEPa and SEPlke) for all $(\mathbf{r}, \mathbf{G})$ as described in the next section.

At large r the adiabatic polarization potential has the asymptotic form

$$V^{\mathrm{Pa}}(\mathbf{r}, \mathbf{G}) \underset{r\to\infty}{\sim} -\alpha_d/(2r^4) .$$

Using the calculated values at $r = 30a_0$ yields $\alpha_d = 15.9a_0^3$, which may be compared to the accurate value[28] of $17.27a_0^3$. The difference of 8% is probably due mainly to correlation effects.

IV. FITTING THE POTENTIAL

For computational purposes we write the potential in three parts

$$V^{SEP}(\mathbf{r}, \mathbf{G}, E) = V^{en}(\mathbf{r}, \mathbf{G}) + V^{eeE}(\mathbf{r}, \mathbf{G}) + V^{P}(\mathbf{r}, \mathbf{G}, E) , \quad (34)$$

where

$$V^{eeE}(\mathbf{r}, \mathbf{G}, E) = V^{ee}(\mathbf{r}, \mathbf{G}) + V^{E}(\mathbf{r}, \mathbf{G}, E) , \quad (35)$$

$V^{ee}(\mathbf{r}, \mathbf{G})$ and $V^{en}(\mathbf{r}, \mathbf{G})$ are the electron–electron and electron–nucleus parts of the static potential, and $V^{P}(\mathbf{r}, \mathbf{G}, E)$ denotes either $V^{\mathrm{Pa}}(\mathbf{r}, \mathbf{G})$ or $V^{\mathrm{Plke}}(\mathbf{r}, \mathbf{G}, E)$.

The electron–nucleus part of the static potential may be calculated analytically as the sum of five Coulomb interactions. If the coordinates of the hydrogen atoms when $\alpha = \beta = \gamma = 0$ are denoted $(R, \theta_{Hk}, \phi_{Hk})$, then the expansion of this contribution in symmetrized harmonics is given by

$$V^{en}(\mathbf{r}, \mathbf{G}) = \sum_{\lambda=0}^{\infty} \sum_{i=1}^{i_{\max}(\lambda)} V_{\lambda i}^{en}(r) T_{\lambda i}(\theta, \phi, \mathbf{G}) , \quad (36)$$

where

$$V_{\lambda i}^{en}(r) = \begin{cases} -\left(\dfrac{6}{r} + \dfrac{4}{r_>}\right)\sqrt{4\pi} , & \lambda = 0 , \\ -\dfrac{4\pi}{2\lambda+1} \dfrac{r_<^{\lambda}}{r_>^{\lambda+1}} \displaystyle\sum_{k=1}^{4} T_{\lambda i}(\theta_{Hk}, \phi_{Hk}, \mathbf{G}) , & \lambda \neq 0 , \end{cases} \quad (37)$$

$$r_< = \min(r, R) , \quad (38)$$

and

$$r_> = \max(r, R) . \quad (39)$$

In practice the sum over λ must be truncated at $\lambda_{\max}$. We found that the sum is very slowly convergent to the sum of the five Coulomb interactions, especially for the electron near a hydrogen nucleus. However, the addition or deletion of a few higher-λ terms has only a small effect on the scattering. For example, the T matrix elements for $J = 0$ differ by only 0.5%–2% for calculations with $\lambda_{\max} = 13$ and 11, which correspond to 12 and 9 terms in the expansion, respectively. Thus, for all production runs we set $\lambda_{\max} = 13$.

$V^{eeE}(\mathbf{r}, \mathbf{G}, E)$ was calculated by subtracting the five Coulomb interactions from $V^{SE}(\mathbf{r}, \mathbf{G})$. It was expanded as

$$V^{eeE}(\mathbf{r}, \mathbf{G}, E) = \sum_{\lambda=0}^{\lambda_{\max}} \sum_{i=1}^{i_{\max}(\lambda)} V_{\lambda i}^{eeE}(r, E) T_{\lambda i}(\theta, \phi, \mathbf{G}) , \quad (40)$$

by retaining N terms on the right-hand side of Eq. (40), substituting N values of $V^{eeE}(\mathbf{r}, \mathbf{G}, E)$, and solving the resulting N simultaneous equations for the first N of the

$V_{\lambda t}^{ee\lambda}(r, E)$. We tried various sets of N points and found that an optimum set must be chosen carefully for an accurate expansion. For N too small the sum is not well converged; for N too large or for the wrong choice of $(\mathbf{r}, \mathbf{G})$ values, the $V_{\lambda t}^{eeE}(r, E)$ are inaccurate, presumably because the differences between some of the included $V^{eeE}(\mathbf{r}, \mathbf{G}, E)$ become relatively small and sensitive to small numerical errors. For the final fits we chose $N=5$ ($\lambda_{max}=7$) for $r=0.1-1.0a_0$ and $3.1-6.4a_0$ and $N=8$ ($\lambda_{max}=10$) for $r=1.3-2.8a_0$. The $N=5$ set was $(\chi, \phi_\chi)=(0,0)$, $(2\tau, 0)$, $(2\tau, 60)$, $(4\tau, 0)$, and $(4\tau, 60)$, and the $N=8$ set consisted of these points plus $(3\tau, 0)$, $(3\tau, 60)$, and $(4\tau, 30)$. A measure of the accuracy of the resulting representation was obtained by using the truncated sums of Eq. (40) to calculate $V^{eeE}(\mathbf{r}, \mathbf{G}, E)$ at points other than the ones used to generate the components $V_{\lambda t}^{eeE}(r, E)$. These checks indicate that the present representation is accurate to 1% or better for $r \leq 1.6a_0$ and $r \geq 2.5a_0$, with a worst error of less than about 5% occurring for the case where the electron is close to an H.

Each resulting $V_{\lambda t}^{eeE}(r, E)$ for $\lambda=0-7$ is represented by the analytic form

$$V_{\lambda t}^{X}(r, E)=c_{\lambda t}^{X} r^{\lambda}+d_{\lambda t}^{X} r^{\lambda+1}, \tag{41}$$

with X = eeE for $r \leq 0.1a_0$, by a 14-node spline fit[30] for $r=0.1-2.044a_0$, where there is a cusp, by another 14-node spline fit for $r=2.044-7.0a_0$, and by

$$V_{01}^{eeE}(r, E)=10(4\pi)^{1/2}/r+f_{01}(E)/r^2+g_{01}(E)/r^3 \tag{42}$$

and

$$V_{\lambda t}^{eeE}(r, E)=e_{\lambda t}(E)/r^{\lambda+1}+f_{\lambda t}(E)/r^{\lambda+2}, \quad \lambda \neq 0, \tag{43}$$

for $r \geq 7.0a_0$. The $V_{\lambda t}^{eeE}(r, E)$ components with $\lambda=8-10$ are set equal to zero for $r \leq 1.0a_0$ and $r \geq 3.1a_0$; each of these components is represented by a five-node spline fit for $r=1.0-2.044a_0$ and by a six-node spline fit for $r=2.044-3.1a_0$.

The adiabatic polarization potential was expanded as

$$V^{Pa}(\mathbf{r}, \mathbf{G})=\sum_{\lambda=0}^{\lambda_{max}} \sum_{t=1}^{t_{max}(\lambda)} V_{\lambda t}^{Pa}(r) T_{\lambda t}(\theta, \phi, \mathbf{G}), \tag{44}$$

with $\lambda_{max}=7$. Each component $V_{\lambda t}^{Pa}(r)$ is represented by Eq. (41) with X = Pa for $r \leq 0.1a_0$, by a 17-node spline fit for $r=0.1-7.0a_0$, and by

$$V_{01}^{X}(r)=-\frac{\alpha_{01} A_{01}^{X}}{2r^4}+\frac{B_{01}^{X}}{r^6}+\frac{C_{01}^{X}}{r^8} \tag{45}$$

and

$$V_{\lambda t}^{X}(r)=\frac{A_{\lambda t}^{X}}{r^{\lambda+2}}+\frac{B_{\lambda t}^{X}}{r^{\lambda+4}}, \quad \lambda \neq 0, \tag{46}$$

with X = Pa and $A_{01}^{Pa}=(4\pi)^{1/2}$ for $r \geq 7.0a_0$. The parameter α_{01} is the spherically averaged static dipole polarizability. For the fit we used our calculated value of $15.9a_0^3$.

Using the above fits to $V^{SE}(\mathbf{r}, \mathbf{G}, E)$ and $V^{Pa}(\mathbf{r}, \mathbf{G})$ we calculated $V^{Plke}(\mathbf{r}, \mathbf{G}, E)$ at the eight (χ, ϕ_χ) values (0, 0), $(2\tau, 0)$, $(2\tau, 60)$, $(3\tau, 0)$, $(3\tau, 60)$, $(4\tau, 0)$, $(4\tau, 30)$, and $(4\tau, 60)$ and fit it by

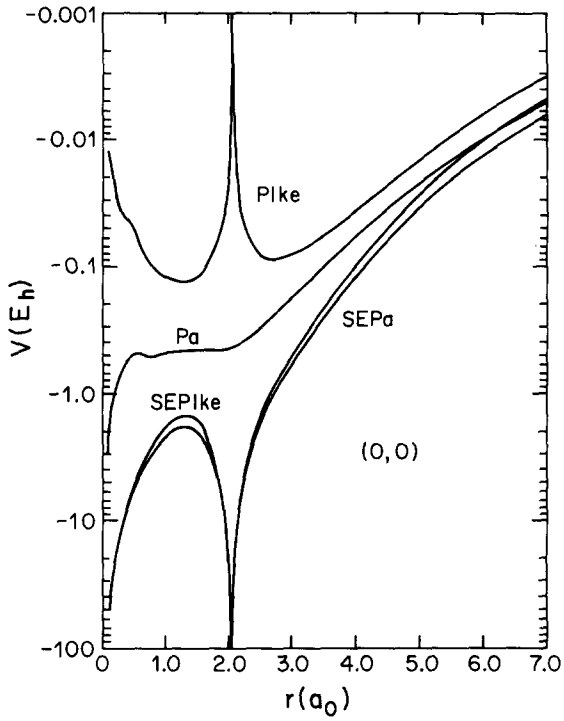

FIG. 1. Polarization and total effective potentials for CH_4 at 10 eV as functions of the radial position of scattering electron for the relative coordinates $(\chi, \phi_\chi)=(0,0)$. Labels are as explained in the text.

$$V^{Plke}(\mathbf{r}, \mathbf{G}, E)=\sum_{\lambda=0}^{\lambda_{max}} \sum_{t=0}^{t_{max}(\lambda)} V_{\lambda t}^{Plke}(r, E) T_{\lambda t}(\theta, \phi, \mathbf{G}), \tag{47}$$

with $\lambda_{max}=10$ for all r. The eight-term expansion has much larger relative errors for $V^{Plke}(\mathbf{r}, \mathbf{G}, E)$ near the nuclei than it has for $V^{eeE}(\mathbf{r}, \mathbf{G}, E)$, but these errors are not very important because $V^{SE}(\mathbf{r}, \mathbf{G}, E)$ dominates $V^{Plke}(\mathbf{r}, \mathbf{G}, E)$ there. Checking the values produced by Eq. (47) at $(\theta, \phi, \mathbf{G})$ values not used for the fit indicates that the error in fitting $V^{Plke}(\mathbf{r}, \mathbf{G}, E)$ is at most about 2% of $V^{SE}(\mathbf{r}, \mathbf{G}, E)$.

The components $V_{\lambda t}^{Plke}(r, E)$ were represented by Eq. (41) with X = Plke for $r \leq 0.1a_0$, by a spline fit with the same nodes as for $V_{\lambda t}^{eeE}(r, E)$ at $r=0.1-7.0a_0$, and by Eqs. (45) and (46) with X = Plke and $A_{01}^{Plke}=(4\pi)^{1/2}(1+E/\Delta)^{-1}$ at $r \geq 7.0a_0$.

Various aspects of the interaction potentials are illustrated in Figs. 1–5. Notice that the adiabatic (Pa) and local kinetic energy nonadiabatic (Plke) polarization potentials differ substantially for $r=0-4a_0$ for all three directions of approach shown in Figs. 1–3; however, the static-exchange part of the effective potential dominates the polarization part at short and intermediate r, so differences between the SEPa and SEPlke are usually less than about 20%. Larger differences occur in the tail region where the polarization potential dominates; in these regions the SEPa effective potential is higher than the SEPlke one by as much as 35%. The λ components of the potentials (Figs. 4 and 5) show cusps at the C–H bond distance. The cusp in the spherical average is

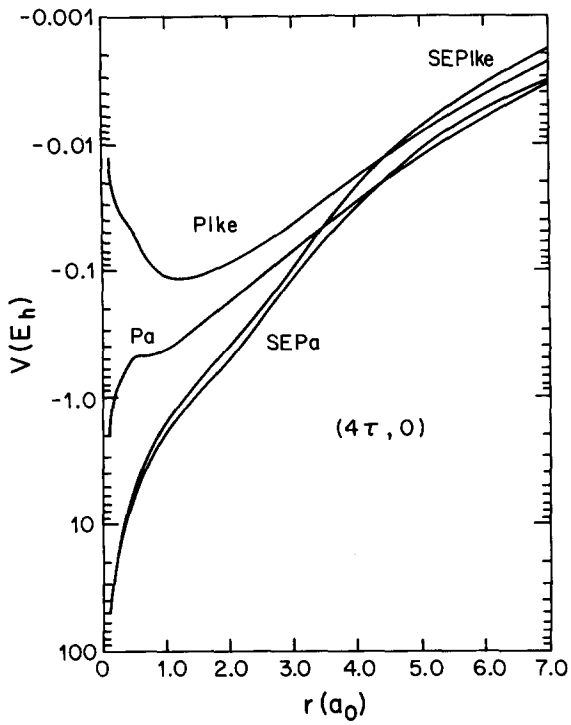

FIG. 2. Polarization and total effective potentials for CH_4 at 10 eV as functions of the radial position of scattering electron for the relative coordinates $(\chi, \phi_\chi) = (4\tau, 0)$. Labels are as explained in the text.

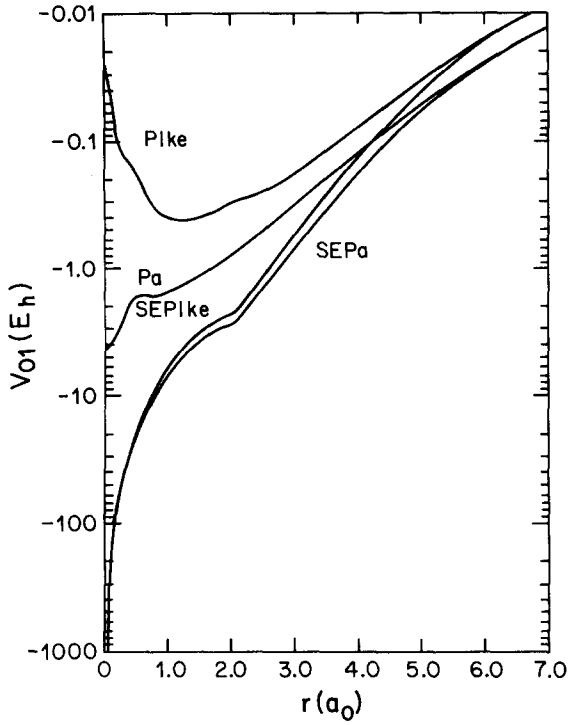

FIG. 4. The $\lambda = 0$ component [equivalent to $(4\pi)^{1/2}$ times the spherical average] of the polarization and total effective potentials for CH_4 at 10 eV as functions of the radial position of the scattering electron. Labels are as explained in the text.

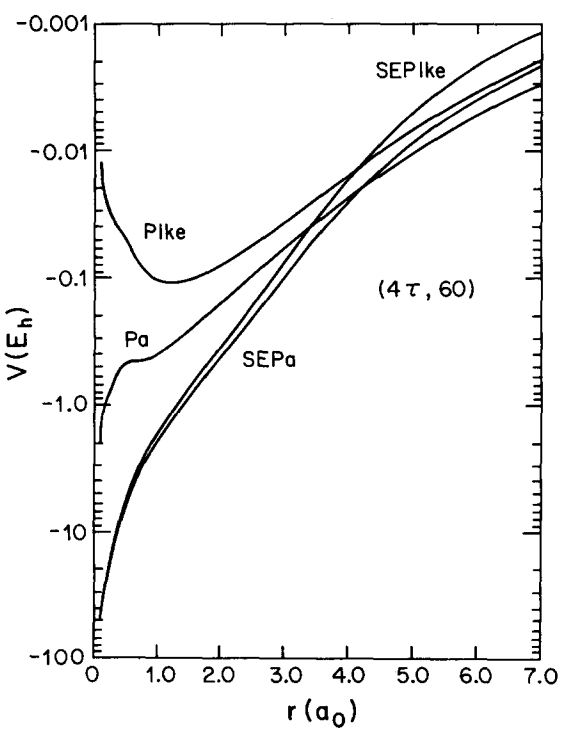

FIG. 3. Polarization and total effective potentials for CH_4 at 10 eV as functions of the radial position of scattering electron for the relative coordinates $(\chi, \phi_\chi) = (4\tau, 60)$. Labels are as explained in the text.

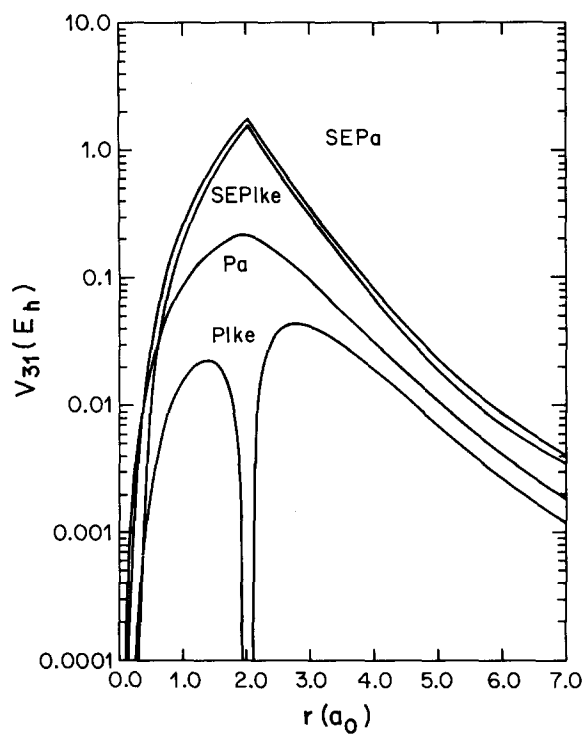

FIG. 5. The first asymmetric $\lambda = 3$ component of the polarization and total effective potentials for CH_4 at 10 eV as functions of the radial position of the scattering electron. Labels are as explained in the text.

TABLE II. Comparison of efficiencies of close coupling codes.

J	Number of channels	Code	Eigenphase sum (mod π)	CPU time (s)[a]
0	2	VIVAS	2.6598	24
		MNN	2.6599	24
0	10	VIVAS	2.9392	75
		MNN	2.9397	126
30	4	VIVAS[b]	6.535×10^{-4}	60
		MNN	6.538×10^{-4}	40

[a]Central processor unit time (in s) for execution in double precision on the University of Minnesota Chemistry Department Digital Equipment Corporation VAX 11/780 computer.
[b]In this case the optimum mode of operation of the VIVAS code was to use the VIVS method over the whole region of integration.

not a very significant feature, but it is quite distinct for $\lambda=3$ and all the higher λ's.

V. NUMERICAL SOLUTION OF THE CLOSE COUPLING EQUATIONS

In order to solve the close coupling equations, the Minnesota Numerov code[31] (MNN, version 80-10A) was used to compute T matrix elements for total angular momenta ranging from $J=0$ to $J=40$. Convergence of the numerical solutions was carefully checked for all integration parameters. The starting point of the numerical integration was increased gradually from $R_0=10^{-5}a_0$ for $J=0$ to $R_0=20a_0$ for $J=40$. The criterion used for large J ($J\geq 11$) was

$$R_0\simeq(l_{\min}/2)a_0\ ,$$

where $l_{\min}$ is the minimum relative angular momentum in any of the coupled channels. The ending point of the integration varied from $R_{\max}=30a_0$ for $J=0$ to $R_{\max}=100a_0$ for $J=40$. The first four steps were carried out with an optimized initial stepsize of $5\times10^{-5}a_0$, then the stepsize was controlled by a variable-stepsize algorithm[31] with a parameter DELTA. For $J\leq 10$ the stepsize was allowed to increase according to the algorithm with no constraint, and it grew as large as $0.4a_0$ in some cases. For $J\geq 11$, an upper limit of $0.064a_0$ had to be enforced to insure good convergence since at large J the solutions become quite sensitive to the accuracy of the large-r integration. The convergence of the solutions relative to the parameter DELTA was monitored for $J=0$, 1, 3, 13, 20, and 30, and DELTA was chosen for other J by generalizing this experience. A typical converged value was DELTA $=-1.5\times10^{-8}$.

There has been interest recently in comparing the performance of various numerical integration schemes for the solution of coupled channel scattering equations. The hybrid variable-interval variable stepsize VIVAS[32] has been judged by Thomas *et al.*[33] to be the most generally efficient code. We made a careful comparison of the efficiency of our Numerov code to that of the VIVAS code[34] (our version 82-2) for the present problem. We carefully optimized both codes to obtain the most efficient integrations consistent with 1% accuracy in the first row of the T matrix. Both codes were optimized with respect to initial and maximum stepsizes and the starting and ending points of the integration. MNN was also optimized with respect to DELTA; VIVAS was also optimized with respect to the switchover from the log derivative (LOGD) method[35] at small r to the variable-interval variable-step (VIVS) method[36] at large r, with respect to the number of steps per interval in VIVS, and with respect to the parameter TOFF that controls the stepsize at which perturbation corrections of the wave function and its derivatives are made in VIVS. The parameters were optimized for a two-channel $J=0$ run and then re-optimized for a four-channel $J=30$ run. The optimized parameters for $J=0$ were also used for a ten-channel run and the resulting T matrix elements in the first row still agreed to 1%. The computation times for these runs are shown in Table II. We conclude that the efficiencies of the two codes are the same within a factor of about 1.7; this is consistent with the conclusion reached by Thomas *et al.*[33] for an electron-N_2 test case.[37] Since the MNN code has less parameters to optimize we found it to be more convenient, and we used MNN for the production runs.

VI. RESULTS

The rotational close coupling calculations were carried out using the laboratory-frame formalism of Sec. II. In this scheme, a basis set of rotational–orbital quantum numbers is determined by specifying a maximum total angular momentum $J_{\max}$ and for every J a maximum rotational quantum number $j_{\max}$. The centrifugal sudden decoupling index n defined by[38]

$$n=l-\max\begin{Bmatrix}|J-j|\\ J\end{Bmatrix}\ , \tag{48}$$

was assigned a maximum value $n_{\max}=2$ for $J\geq 4$, but for $J=0$–3 it was not restricted beyond the limitations imposed by $j_{\max}$. Convergence with respect to $n_{\max}$ was checked at $J=3$ with $j_{\max}=11$ and at $J=10$ with $j_{\max}=7$. The first row T matrix elements changed by only 0.5%–2.0% as $n_{\max}$ was changed from two to three and by 1.0%–3.0% as $n_{\max}$ was changed from two to ∞, with the least errors made in the largest elements. Thus, the limitation on $n_{\max}$ causes negligible truncation error in these tests. These tests are actually more strict than required for our procedure since we always converge with respect to $j_{\max}$ at a given $n_{\max}$.

In order to illustrate the overall degree of convergence relative to $J_{\max}$, $j_{\max}$, and the number of channels N, results for the SEPa potential will be presented for three basis sets (to be called I, II, and III). The maximum rotational angular momentum quantum numbers $j_{\max}$, the number of channels N, and the CPU time on the VAX 11/780 computer are tabulated for each total angular momentum J or range of J. The criterion for constructing basis III was that the larger first-row T matrix elements are converged to 1% or better and that relative errors in less important first-row elements do not exceed 3%. The other bases are used only for demonstrating convergence.

TABLE III. Basis sets for electron-methane scattering.

	Basis I			Basis II			Basis III		
J	$j_{max}(J)$	N	CPU (min)	$j_{max}(J)$	N	CPU (min)	$j_{max}(J)$	N	CPU (min)
0	12[a]	10	3.5	12[a]	10	3.5	13[b]	12	11.9
1	11	17	13.5	11	17	13.5	12[a]	19	40.9
2	10	22	26.6	10	22	26.6	11	25	41.4
3	9	25	28.4	10	29	64.3	11	33	66.7
4[c]	9	19	7.4	10	24	15.8	11	28	27.0
5	9	20	8.5	10	22	10.9	11	27	22.0
6	9	24	16.0	9	24	16.0	10	27	22.3
7	8	23	14.1	8	23	14.1	9	27	21.8
8	6	13	3.7	7	18	9.0	8	24	19.7
9	6	13	4.1	7	18	9.8	8	24	20.8
10	6	13	4.1	6	13	4.1	7	18	9.6
11–19	6	13	45.0	6	13	45.0	6	13	45.0
20	4	8	1.9	4	8	1.9	6	13	5.7
21–29	4	8	18.0	4	8	18.0	4	8	18.0
30	0	1	0.4	3	4	0.7	4	8	2.0
31–35	...	0	...	0	1	1.9	3	4	3.3
36–40	...	0	...	...	0	...	0	1	2.0
Total CPU (min)			195			255			380

[a]This includes only the first $j = 12$ basis function, i.e., the one for which $\langle jk | jp\mu h \rangle$ is nonzero for $k = 0$.
[b]This includes both $j = 12$ basis functions.
[c]For $J \leq 3$, there is no limit on the centrifugal sudden decoupling index n. For $J \geq 4$, $n_{max} = 2$.

Assuming that the molecule is initially in its electronic and rotational ground state, the first-row T matrix elements obtained from the numerical solution of the coupled differential equations were used to compute state-to-state rotationally elastic and inelastic integral cross sections $\sigma_{0j'}$, momentum transfer cross sections $\sigma^m_{0j'}$, and differential cross sections $(d\sigma_{0j'}/d\Omega)(\theta)$. These cross sections were summed over j' ($j' = 0$–11) to obtain the (electronically and vibrationally elastic) rotationally summed cross sections σ_0, σ^m_0, and $(d\sigma_0/d\Omega)(\theta)$, respectively.

State-to-state and vibrationally elastic differential cross sections obtained using the three bases of Table III are given in Table IV for the SEPa potential and all three scattering bases at four scattering angles, and in Tables V and VI for the SEPa and SEPlke potentials and basis III at 21 scattering angles. Basis III is our largest and consequently most converged basis set. The SEPa and SEPlke rotationally elastic ($j = 0, 0 \rightarrow 0$) and the largest rotationally inelastic ($0 \rightarrow j'$) differential cross sections are compared in Fig. 6; while the rotationally summed differential cross sections are compared in Fig. 7 to each other, to experiment,[4–6] and to other theoretical results.[8]

In Table VII, the SEPa integral and momentum transfer cross sections obtained using the three bases are compared to one another and to the corresponding SEPlke cross sections obtained with basis III. Table

TABLE IV. State-to-state and vibrationally elastic differential cross sections (a_0^2/sr) at selected scattering angles, using the SEPa potential.

θ		$d\sigma_{0j'}/d\Omega$							$\frac{d\sigma_0}{d\Omega}$
(deg)	Basis	$j' = 0$	3	4	6	7	8	9	
0	I	4.07(+1)	5.78(−4)	1.04	7.62(−3)	8.15(−6)	6.94(−7)	4.80(−8)	4.17(+1)
	II	4.09(+1)	6.63(−4)	1.04	8.03(−3)	9.43(−6)	7.31(−7)	4.62(−8)	4.19(+1)
	III	4.11(+1)	5.38(−4)	1.04	8.18(−3)	9.18(−6)	8.21(−7)	4.51(−8)	4.22(+1)
60	I	2.26	1.12	1.10	3.50(−3)	3.01(−4)	1.95(−6)	1.57(−7)	4.49
	II	2.25	1.12	1.10	3.70(−3)	3.21(−4)	2.10(−6)	1.68(−7)	4.48
	III	2.26	1.13	1.10	3.77(−3)	3.27(−4)	2.23(−6)	1.54(−7)	4.50
120	I	8.99(−2)	4.04(−1)	1.11	1.30(−2)	4.54(−4)	2.48(−6)	2.34(−7)	1.61
	II	8.70(−2)	4.05(−1)	1.11	1.35(−2)	4.85(−4)	2.60(−6)	2.57(−7)	1.61
	III	9.01(−2)	4.04(−1)	1.11	1.36(−2)	4.94(−4)	2.86(−2)	2.19(−7)	1.62
180	I	1.74(+1)	5.05(−1)	1.55	3.48(−2)	1.34(−3)	4.26(−6)	2.52(−6)	1.95(+1)
	II	1.74(+1)	5.18(−1)	1.55	3.61(−2)	1.40(−3)	4.55(−6)	2.67(−6)	1.95(+1)
	III	1.73(+1)	5.14(−1)	1.55	3.63(−2)	1.43(−3)	4.91(−6)	3.27(−6)	1.94(+1)

TABLE V. State-to-state and vibrationally elastic differnetial cross sections (a_0^2/sr) at selected scattering angles, using basis III and the SEPa potential.

θ (deg)	$d\sigma_{0j'}/d\Omega$							$\frac{d\sigma_0}{d\Omega}$
	$j'=0$	3	4	6	7	8	9	
0	4.11(+1)	5.38(−4)	1.04	8.18(−3)	9.18(−6)	8.21(−7)	4.51(−8)	4.22(+1)
5	3.69(+1)	1.65(−2)	1.04	8.12(−3)	1.34(−5)	8.16(−7)	4.74(−8)	3.79(+1)
10	3.10(+1)	6.73(−2)	1.045	7.95(−3)	2.59(−5)	8.06(−7)	5.42(−8)	3.21(+1)
15	2.57(+1)	1.49(−1)	1.05	7.68(−3)	4.59(−5)	7.96(−7)	6.48(−8)	2.69(+1)
20	2.08(+1)	2.57(−1)	1.06	7.32(−3)	7.26(−5)	7.97(−7)	7.81(−8)	2.22(+1)
30	1.27(+1)	5.15(−1)	1.08	6.41(−3)	1.40(−4)	8.77(−7)	1.08(−7)	1.43(+1)
40	6.80	7.75(−1)	1.09	5.40(−3)	2.14(−4)	1.13(−6)	1.35(−7)	8.67
50	3.44	9.89(−1)	1.10	4.47(−3)	2.80(−4)	1.60(−6)	1.51(−7)	5.54
60	2.26	1.13	1.105	3.77(−3)	3.27(−4)	2.23(−6)	1.54(−7)	4.50
70	2.35	1.17	1.10	3.48(−3)	3.49(−4)	2.88(−6)	1.42(−7)	4.62
80	2.80	1.11	1.09	3.76(−3)	3.51(−4)	3.39(−6)	1.14(−7)	4.80
90	2.72	9.73(−1)	1.075	4.79(−3)	3.46(−4)	3.62(−6)	7.65(−8)	4.78
100	1.88	7.85(−1)	1.07	6.73(−3)	3.55(−4)	3.53(−6)	5.00(−8)	3.74
110	7.07(−1)	5.82(−1)	1.08	9.67(−3)	3.99(−4)	3.21(−6)	7.62(−8)	2.38
120	9.01(−2)	4.04(−1)	1.11	1.36(−2)	4.94(−4)	2.86(−6)	2.19(−7)	1.62
130	9.30(−2)	2.86(−1)	1.17	1.83(−2)	6.44(−4)	2.70(−6)	5.45(−7)	2.41
140	3.64	2.52(−2)	1.26	2.34(−2)	8.39(−4)	2.88(−6)	1.08(−6)	5.17
150	7.85	2.99(−1)	1.36	2.84(−2)	1.05(−3)	3.40(−6)	1.79(−6)	9.54
160	1.25(+1)	3.92(−1)	1.45	3.26(−2)	1.24(−3)	4.09(−6)	2.51(−6)	1.43(+1)
170	1.60(+1)	4.79(−1)	1.53	3.53(−2)	1.38(−3)	4.68(−6)	3.07(−6)	1.80(+1)
180	1.73(+1)	5.14(−1)	1.55	3.63(−2)	1.43(−3)	4.91(−6)	3.27(−6)	1.94(+1)

VIII gives the partial wave contributions q_l to the integral state-to-state and rotationally summed cross sections. Elastic and momentum transfer cross sections are compared to experiment[5,39,40] and to other theories[7,41] in Table IX. Finally, in Table X we compare the various experimental[5,6] and theoretical[8] values of the ratio of $(d\sigma_0/d\Omega)(\theta)$ to $(d\sigma_0/d\Omega)(\theta' \neq 0)$; our own results in this table are for basis III.

The two previous theoretical studies to which we compare are those of Buckingham *et al.*[41] and Gianturco and Thompson.[7,8] Buckingham *et al.* made a spherical average of the proton field of CH_4 to obtain central-field SCF orbitals. They then calculated the integral cross section by phase shifts for the resulting static potential. The Gianturco–Thompson calculation is more in the spirit of the present results. However, it is less com-

TABLE VI. State-to-state and vibrationally elastic differential cross sections (a_0^2/sr) at selected scattering angles, using basis III and the SEPlke potential.

θ (deg)	$d\sigma_{0j'}/d\Omega$							$\frac{d\sigma_0}{d\Omega}$
	$j'=0$	3	4	6	7	8	9	
0	5.04(+1)	1.22(−4)	6.05(−1)	1.24(−3)	4.73(−7)	4.60(−7)	7.16(−9)	5.10(+1)
5	4.73(+1)	5.58(−3)	6.05(−1)	1.22(−3)	1.93(−6)	4.52(−7)	7.26(−9)	4.79(+1)
10	4.22(+1)	2.25(−2)	6.05(−1)	1.19(−3)	6.21(−6)	4.28(−7)	7.56(−9)	4.29(+1)
15	3.68(+1)	4.92(−2)	6.05(−1)	1.13(−3)	1.30(−5)	3.93(−7)	8.05(−9)	3.74(+1)
20	3.12(+1)	8.48(−2)	6.04(−1)	1.06(−3)	2.19(−5)	3.53(−7)	8.72(−9)	3.19(+1)
30	2.06(+1)	1.73(−1)	6.02(−1)	8.89(−4)	4.35(−5)	2.85(−7)	1.06(−8)	2.14(+1)
40	1.24(+1)	2.67(−1)	5.98(−1)	7.20(−4)	6.62(−5)	2.77(−7)	1.32(−8)	1.33(+1)
50	7.32	3.50(−1)	5.90(−1)	6.19(−4)	8.50(−5)	3.58(−7)	1.63(−8)	8.26
60	4.85	4.02(−1)	5.80(−1)	6.63(−4)	9.75(−5)	5.20(−7)	1.88(−8)	5.84
70	3.88	4.10(−1)	5.69(−1)	9.40(−4)	1.05(−4)	7.20(−7)	1.87(−8)	4.86
80	3.27	3.70(−1)	5.55(−1)	1.54(−3)	1.13(−4)	9.08(−7)	1.49(−8)	4.20
90	2.36	2.93(−1)	5.42(−1)	2.53(−3)	1.31(−4)	1.06(−6)	1.08(−8)	3.20
100	1.17	2.03(−1)	5.31(−1)	3.96(−3)	1.73(−4)	1.19(−6)	2.01(−8)	1.90
110	2.51(−1)	1.30(−1)	5.23(−1)	5.83(−3)	2.49(−4)	1.37(−6)	6.97(−8)	9.10(−1)
120	3.79(−1)	1.03(−1)	5.20(−1)	8.06(−3)	3.64(−4)	1.69(−6)	1.97(−7)	1.01
130	2.10	1.41(−1)	5.25(−1)	1.05(−2)	5.17(−4)	2.23(−6)	4.36(−7)	2.78
140	5.46	2.45(−1)	5.38(−1)	1.30(−2)	6.93(−4)	2.98(−6)	7.95(−7)	6.25
150	9.86	3.95(−1)	5.57(−1)	1.53(−2)	8.72(−4)	3.86(−6)	1.24(−6)	1.08(+1)
160	1.43(+1)	5.54(−1)	5.77(−1)	1.72(−2)	1.03(−3)	4.70(−6)	1.68(−6)	1.54(+1)
170	1.76(+1)	6.75(−1)	5.92(−1)	1.84(−2)	1.13(−3)	5.31(−6)	2.01(−6)	1.88(+1)
180	1.88(+1)	7.20(−1)	5.98(−1)	1.88(−2)	2.13(−6)	5.53(−6)	2.13(−6)	2.01(+1)

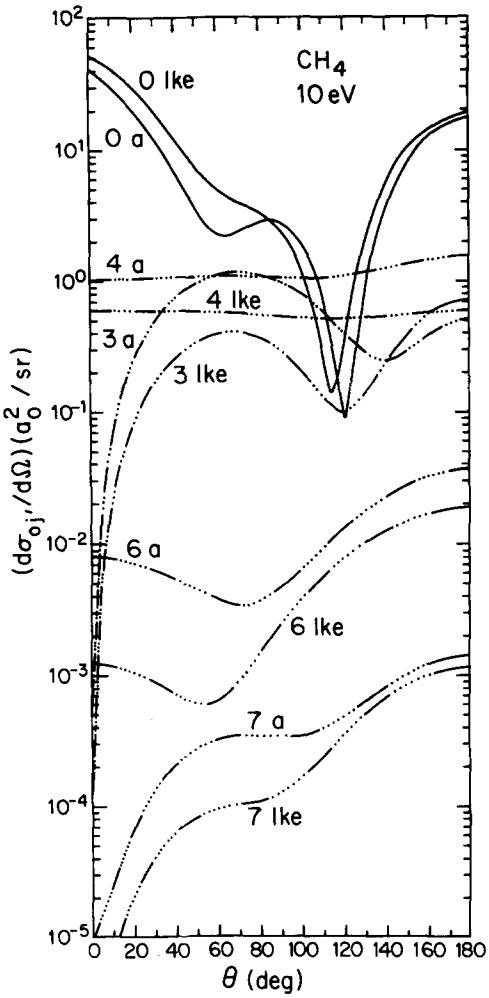

FIG. 6. Differential cross sections for pure elastic scattering (labeled 0 a or 0 Ike where a and Ike specify which polarization potential has been used) and state-to-state rotational excitation for $j=0\rightarrow j'=3$, 4, 6, and 7 as functions of the scattering angle These cross sections were calculated with basis III.

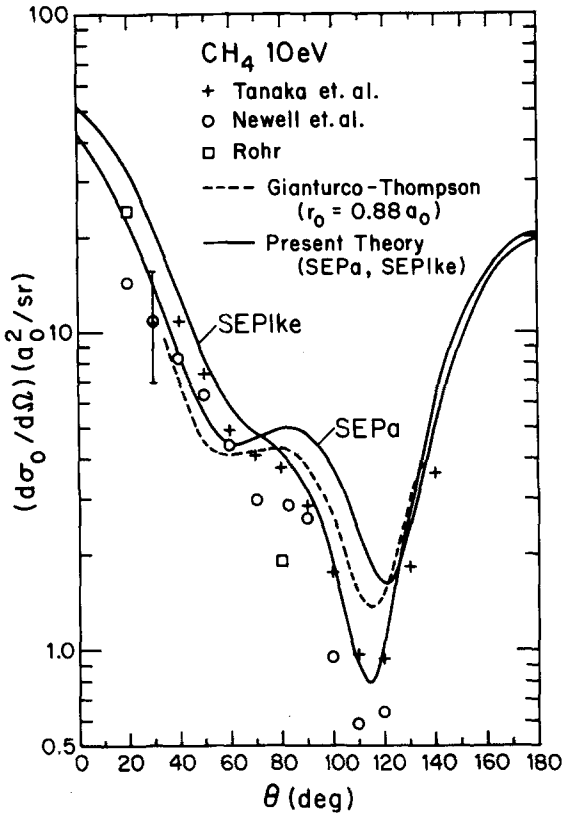

FIG. 7. Electronically and vibrationally elastic, rotationally, summed differential cross sections as functions of the scattering angle for CH_4. The solid curves labeled SEPa and SEPIke represent calculations made with basis III. The dashed curve is the calculation of Gianturco *et al.* (Ref. 8) with their empirical parameter set equal to $0.88a_0$. The experimental results are shown as symbols. All results are for 10 eV except those of Gianturco and Thompson, which are for 9.5 eV.

plete in several ways. Instead of an exchange potential they used an orthogonalization procedure. Instead of an *ab initio* polarization potential they used the spherical approximation given by

$$V^P(r) = -(\alpha/2r^4)\{1-\exp[-(r/r_0)]\}^6 . \quad (49)$$

Both the form of Eq. (49) and the parameter r_0 were chosen by comparison of the scattering results to experiment. In the expansion of the static potential they

TABLE VII. Integral and momentum transfer state-to-state, rotationally inelastic, and vibrationally elastic cross sections (a_0^2).

		SEPa			SEPIke
	j'	Basis I	Basis II	Basis III	Basis III
$\sigma_{0j'}$	0	5.83(+1)	5.82(+1)	5.81(+1)	8.34(+1)
	3	8.93	8.96	8.96	3.44
	4	1.42(+1)	1.42(+1)	1.42(+1)	7.00
	6	1.23(−1)	1.28(−1)	1.29(−1)	6.28(−2)
	7	5.22(−3)	5.55(−3)	5.65(−3)	3.43(−3)
	8	2.99(−5)	3.17(−5)	3.43(−5)	1.75(−5)
	9	4.29(−6)	4.60(−6)	4.94(−6)	3.03(−6)
	10	4.52(−9)	1.03(−7)	1.54(−7)	1.07(−7)
	3–10	2.32(+1)	2.33(+1)	2.33(+1)	1.05(+1)
	0–10	8.15(+1)	8.15(+1)	8.14(+1)	9.39(+1)
$\sigma^m_{0j'}$	0	4.49(+1)	4.49(+1)	4.48(+1)	5.68(+1)
	3–10	2.26(+1)	2.26(+1)	2.26(+1)	1.04(+1)
	0–10	6.75(+1)	6.75(+1)	6.74(+1)	6.72(+1)

TABLE VIII. Partial wave contributions $q_l(a_0^2)$ to the integral cross sections of Table VII (Basis III).

l \ j'	0	3	4	6	7	3–10	0–10
0	5.47[a]	1.24	2.97(−2)	3.15(−5)	5.60(−7)	1.27	6.74
	1.46(+1)[b]	3.88(−1)	9.82(−3)	9.88(−6)	1.40(−7)	3.98(−1)	1.50(+1)
1	1.31	1.96	5.12(−2)	5.54(−5)	1.81(−6)	2.01	3.32
	1.62(+1)	2.35(−2)	6.50(−3)	1.75(−5)	2.22(−7)	3.00(−2)	1.62(+1)
2	4.52(+1)	3.11	1.38(+1)	2.15(−2)	7.53(−4)	1.69(+1)	6.21(+1)
	4.94(+1)	1.26	6.85	1.30(−2)	4.23(−4)	8.12	5.75(+1)
3	5.00	2.52	3.18(−1)	7.89(−2)	2.35(−3)	2.92	7.92
	2.73	1.69	1.02(−1)	3.51(−2)	1.33(−3)	1.83	4.56
4	7.40(−1)	1.15(−1)	4.11(−2)	2.84(−2)	1.88(−3)	1.87(−1)	9.27(−1)
	3.32(−1)	7.28(−2)	2.92(−2)	1.45(−2)	1.27(−3)	1.18(−1)	4.50(−1)
5	2.02(−1)	1.05(−2)	1.13(−3)	1.50(−4)	6.54(−4)	1.24(−2)	2.15(−1)
	8.29(−2)	1.04(−2)	1.01(−3)	6.50(−5)	4.04(−4)	1.19(−2)	9.48(−2)
6	8.04(−2)	3.24(−3)	1.50(−4)	4.07(−5)	6.57(−6)	3.44(−3)	8.38(−2)
	3.13(−2)	2.30(−3)	1.44(−4)	3.24(−5)	2.95(−6)	2.48(−3)	3.38(−2)
7	3.45(−2)	1.07(−3)	3.71(−5)	1.32(−6)	9.50(−7)	1.11(−3)	3.56(−2)
	1.45(−2)	7.91(−4)	2.90(−5)	9.20(−7)	5.22(−7)	8.21(−4)	1.53(−2)
8	2.20(−2)	4.59(−4)	1.0(−5)	7.0(−8)	7.4(−8)	4.69(−4)	2.25(−2)
	7.65(−3)	3.56(−4)	8.0(−6)	7.0(−8)	5.4(−8)	3.64(−4)	8.02(−3)
9	1.37(−2)	2.30(−4)	3.1(−6)	4.0(−8)	1.9(−8)	2.33(−4)	1.39(−2)
	4.41(−3)	1.84(−4)	2.0(−6)	2.0(−8)	1.4(−8)	1.86(−4)	4.60(−3)
10–40	2.12(−2)	3.53(−4)	7.0(−7)	2.0(−8)	2.5(−8)	3.53(−4)	2.16(−2)
	7.59(−3)	2.99(−4)	2.0(−6)	2.0(−8)	5.0(−9)	3.01(−4)	7.89(−3)
0–40	5.81(+1)	8.96	1.42(+1)	1.29(−1)	5.65(−3)	2.33(+1)	8.14(+1)
	8.34(+1)	3.44	7.00	6.28(−2)	3.43(−3)	1.05(+1)	9.39(+1)

[a]Upper entry: SEPa. [b]Lower entry: SEPlke.

used five terms as compared to eight or 12 terms for parts of the present potential. They used a body-frame treatment of the scattering involving four symmetries with five coupled channels each. A converged body-frame treatment, which would be equivalent to a converged space-frame treatment such as employed here, would involve five symmetries and more coupled channels per symmetry.

VII. DISCUSSION AND COMPARISON TO EXPERIMENT

Tables IV and VII show that the rotationally summed SEPa differential, integral, and momentum transfer cross sections are converged to better than 1.5% in most cases. The convergence of the state-to-state integral cross sections for $j' \geq 7$ and the state-to-state differential cross sections for $j' \geq 3$ is not as good, but we note that the worse relative errors occur in comparatively small state-to-state cross sections, and the convergence of the important cross sections is acceptable. We also note that the $j = 0 \rightarrow j' = 10$ or 11 cross sections were of negligible magnitude and poorly converged, hence we chose not to report them in any of Tables IV–VIII.

As discussed at the end of Sec. IV, the differences between the SEPa and SEPlke effective potentials are not large. Nevertheless, the scattering is quite sensitive to the choice of potential, especially for low total angular momenta ($J = 0$–3). This is most clear in the partial cross sections of Table VIII and in the changes

TABLE IX. Electronically and vibrationally elastic, rotationally summed integral and momentum-transfer cross sections (a_0^2) at 10 eV.

Authors	σ_0	σ_0^m	Reference
Experiment			
Kieffer (review)	84		39
Barbarito *et al.*	60 ± 7[a]	...	40
Tanaka *et al.*	66 ± 8[b]	47 ± 6[b]	5
Theory			
Buckingham, Massey, and Tibbs	64	c	41
Gianturco and Thompson ($r_0 = 0.84a_0$)	76	c	7
Present work SEPa (basis III)	81	67	...
Present work SEPlke (basis III)	94	67	...

[a]Theee standard deviations of measured integral cross section.
[b]Propagated standard deviations of differential cross section measurements; integral cross sections then calculated by fitting, extrapolating, and integrating.
[c]Not available.

TABLE X. Comparison between theoretical and experimental ratios of differential cross sections at 10 eV at different scattering angles.

		$d\sigma/d\Delta(\theta)$; $d\sigma/d\Omega(\theta')$				
Authors	θ/θ'	30/90	40/90	60/90	60/120	Reference
Experiment						
Newell *et al.*		4.4	3.2	1.7	6.9	6
Tanaka *et al.*						
measurement		3.9	3.8	1.7	5.3	5
fit		4.4	3.3	2.1	6.2	
Theory						
Gianturco and Thompson						
$r_0 = 0.84a_0$		a	1.5	0.6	1.1	8
$r_0 = 0.88a_0$		a	1.9	1.1	2.7	
$r_0 = 0.92a_0$		a	2.1	1.5	9.5	
Present work						
SEPa		3.0	1.8	0.9	2.8	...
SEPlke		6.7	4.2	1.8	5.8	

[a]Not available.

in the cross sections of Gianturco and Thompson when their empirical parameter is changed by only $0.04a_0$; these changes are illustrated in Table X. Tables V–VIII and Figs. 6 and 7 all illustrate that the rotationally summed cross sections are less sensitive to the choice of potential than are the individual state-to-state cross sections. The nonadiabatic SEPlke potential is the theoretically best justified one, and the results for the SEPa potential are presented only for reference and to test how important the nonadiabatic corrections are. It is encouraging therefore that Fig. 7 shows the SEPlke results to be in excellent agreement with the experimental rotationally summed differential cross sections. This agreement is also exhibited in the ratios of differential cross sections in Table X. The SEPa results are also in qualitative agreement with experiment, but the agreement is definitely worse than for the SEPlke results. While the rotationally summed cross sections for the two potentials are similar, Tables V–VIII and Fig. 6 show that SEPa scattering is much less elastic. Both the agreement of rotationally summed cross sections with experiment and the theoretical reasonableness of the model favor the SEPlke results. Thus, the SEPlke results are the final predicted values of this study, and in particular we believe that the SEPlke rotationally inelastic cross section of $10.5a_0^2$ is a more reliable prediction than the SEPa rotationally inelastic cross section of $23.3a_0^2$. No experiments that resolve j' are available yet for CH_4.

The proper choice of the potential deserves a further comment. Although it is well established in the literature[42] that the adiabatic polarization potential is too attractive, there have been only a few studies that incorporate nonadiabatic effects in a nonempirical way. Since the target does not have infinite time to respond to the field of the incident electron, and since the time available depends on the local kinetic energy of the incident electron, a realistic local approximation to the polarization potential should be explicitly energy dependent. However, the usual practice has been to use energy-independent empirical cutoff parameters to account for nonadiabatic results. Not only is this practice unsatisfactory from a fundamental point of view, but also the scattering results can be very sensitive to the parameter. Table X shows that the ratio of the differential cross section at 60° to its value at 120° computed by Gianturco and Thompson changes by nearly an order of magnitude when the parameter r_0 is changed by 9.5%. In previous work[10] we have successfully used semiempirical minimum-basis-set calculations to compute polarization potentials, and we have obtained good scattering results for a variety of systems at several energies. The minimum-basis-set restriction in these calculations mimics the nonadiabatic effects by not letting the target completely relax to its minimum energy configuration. The present treatment involves a less empirical procedure for diminishing the adiabatic response of the target, namely the semiclassical local kinetic energy approximation derived from a formal expansion of the exact optical potential.[11] As discussed in the previous paragraph, it is gratifying that this *ab initio* model is so successful.

It is mentioned above that the largest differences between the scattering results for the adiabatic and nonadiabatic potentials are in the s, p, d, and f waves. The last column of Table VIII shows that d-wave scattering dominates for both potentials, contributing 76% for the SEPa potential and 61% for the SEPlke potential; this accounts for the d-wave dominated shapes of the rotationally summed differential cross sections in Fig. 7. Pure d-wave scattering would have local minima at 55° and 125° and a local maximum at 90°. The results for the SEPa potential actually show two local minima and a local maximum, but in the experimental results and SEPlke results the first local minimum is replaced by a shoulder due to the larger contributions from other partial waves. The SEPlke results also show a deeper local minimum than the SEPa results at large angles, and again this is in better agreement with the most recent experiments. These shape features of the differen-

tial cross sections are summarized in Table X, which shows that our SEPlke results are within the experimental range for the shape of the differential cross section at 40°–120°. This table also shows the great sensitivity (mentioned above) of the Gianturco–Thompson results to small variations in their empirical parameter. (The value of this parameter used for Fig. 7 was chosen to maximize agreement with experiment.) This great sensitivity of the shape of the rotationally summed differential cross section makes the good agreement of the present nonempirical SEPlke results even more satisfying.

The comparisons of integral cross sections in Table IX are harder to interpret because the experimental result of Tanaka includes an extrapolated contribution from the small-angle scattering that they did not measure. The error estimate of the integral cross section given by Tanaka *et al.*[5] and given in Table IX is stated by them to include only the uncertainty due to the precision of their individual measurements of $d\sigma_0/d\Omega$. It does not include the other errors that affect their value of σ_0, in particular the quality of the fit and the extrapolation used to compute σ_0 by integration. Their extrapolation would appear to be particularly sensitive to error in this case because of the large (38%) uncertainty at 10 eV of their differential cross section at the smallest scattering angle (30°) for which they measured it. A further indication of the uncertainty of the 30° measurement is provided by the 30/90 column of Table X; this column shows a large discrepancy between the measurement of Tanaka *et al.*[5] at 30° and their fit at this angle. The uncertainty in the small-angle experimental differential cross section and in the extrapolation of this cross section to compute the integral cross section explains why the SEPlke differential cross section agrees better with the Tanaka *et al.*[5] measurement than the SEPlke integral cross section agrees with the integral cross section they calculated from their measurements. Nevertheless, it is disturbing that the present calculation of the integral cross section also exceeds the recent direct measurement of Barbarito *et al.* Both the Barbarito *et al.*[40] value and the Tanaka *et al.*[5] value are considerably lower than the values obtained in the older (1927–1930) measurements reviewed by Kieffer.[39] The comparison to Ref. 40 may indicate that the forward peak in the elastic differential cross sections predicted by both potentials studied here is too large.

In summary, we have presented an *ab initio* calculation of electron-methane cross sections at 10 eV using energy-dependent local potentials. We have used the full molecular symmetry of the target to reduce the number of coupled channels in the scattering calculations. The calculated differential cross sections for the effective potential based on the nonadiabatic semiclassical local kinetic energy polarization potential are in good agreement with experimentally measured results for electronically and vibrationally elastic scattering for a wide range of scattering angles (40°–140°). The results are consistent with the importance of nonadiabatic effects even at low energy. It remains an open problem to resolve the apparent discrepancy in the calculated and apparent experimental cross sections for small scattering angles ($\theta \leq 30°$).

ACKNOWLEDGMENTS

We are grateful to Don Secrest for several discussions of his Ar–CH_4 calculations, to Alden Mead for additional discussions, to Hiroshi Tanaka for sending his experimental results prior to publication, to Sandor Trajmar for additional assistance in making the comparison to experiment, and to Thom Dunning and David Weil for assistance with the NYU properties program. This work was supported in part by the National Science Foundation under Grant No. CHE80-25232 and by a grant to D.G.T. and D.A.D. from the National Resounce for Computation in Chemistry. This work was also supported in part by the Director, Office of Energy Research, Office of Basic Energy Sciences, Chemical Sciences Division of the U. S. Department of Energy under Contract No. DE-AC03-76SF00098 and by the National Science Foundation under Grant No. CHE-7721305.

[1]N. F. Lane, Rev. Mod. Phys. 52, 29 (1980).
[2]P. G. Burke, N. Chandra, and F. A. Gianturco, J. Phys. B 5, 2212 (1972).
[3]M. E. Riley and D. G. Truhlar, J. Chem. Phys. 63, 2182 (1975).
[4]K. Rohr, J. Phys. B 13, 4897 (1980).
[5]H. Tanaka, T. Okada, L. Boseten, T. Suzuki, and M. Kubo, J. Phys. B 15, 3305 (1982).
[6]W. R. Newell, D. F. C. Brewer, and A. C. Smith, XIth International Conference on Electronic and Atomic Collisions, Abstracts (Kyoto), 308 (1979).
[7]F. A. Gianturco and D. G. Thompson, J. Phys. B 9, L383 (1976).
[8]F. A. Gianturco and D. G. Thompson, J. Phys. B 13, 613 (1980).
[9]For other recent theoretical work on e^-–CH_4 scattering see (a) Z. Varga, I. Gyemant, and M. G. Benedict, Acta Phys. Chem. 25, 85 (1979); (b) S. Salvini and D. G. Thompson, J. Phys. B 14, 3797 (1981).
[10]For reviews, see (a) D. G. Thuhlar, K. Onda, R. A. Eades, and D. A. Dixon, Int. J. Quantum Chem. Symp. 13, 601 (1979); (b) D. G. Truhlar, in *Chemical Applications of Atomic and Molecular Electrostatic Potentials*, edited by P. Politzer and D. G. Truhlar (Plenum, New York, 1981), p. 123. For more recent work, see (c) D. Thirumalai, K. Onda, and D. G. Truhlar, J. Chem. Phys. 74, 526, 6792 (1981); D. Thirumalai and D. G. Truhlar, *ibid.* 75, 5207 (1981).
[11]S. M. Valone, D. G. Truhlar, and D. Thirumalai, Phys. Rev. A 25, 3003 (1982).
[12]T. Heil and D. Secrest, J. Chem. Phys. 69, 219 (1978); L. N. Smith and D. Secrest, *ibid.* 74, 3882 (1981).
[13]A. R. Edmonds, *Angular Momentum in Quantum Mechanics* (Princeton University, Princeton, 1957). In the present article we follow the conventions of this book for all angular functions and angular momentum coupling coefficients.
[14]S. L. Altmann and A. P. Cracknell, Rev. Mod. Phys. 37, 19 (1965). The decomposition of the CH_4 rotational basis has also been considered by E. B. Wilson, J. Chem. Phys. 3, 276 (1935).
[15]L. D. Landau and E. M. Lifshitz, *Quantum Mechanics: Non-Relativistic Theory*, 2nd ed. (Addison–Wesley, Reading, Mass., 1965), p. 362.
[16]J. M. Blatt and L. C. Biedenharn, Rev. Mod. Phys. 24, 258 (1952).
[17]Because of the phase convention adopted in Eq. (2) and for reasons discussed in D. G. Truhlar, C. A. Mead, and M. A.

Brandt, Adv. Chem. Phys. 33, 296 (1975), it is appropriate to use the Z coefficients of Ref. 16 rather than the $\bar{Z}$ coefficients of A. M. Lane and R. G. Thomas, Rev. Mod. Phys. 30, 257 (1958).

[18]K. Scanlon, R. A. Eades, D. A. Dixon, and J. Overend, J. Phys. Chem. 85, 2878 (1981).

[19](a) R. A. Eades, D. G. Truhlar, and D. A. Dixon, Phys. Rev. A 20, 867 (1979); (b) C. H. Douglass, Jr., D. A. Weil, P. A. Charlier, R. A. Eades, D. G. Truhlar, and D. A. Dixon, in *Chemical Applications of Atomic and Molecular Electrostatic Potentials*, edited by P. Politzer and D. G. Truhlar (Plenum, New York, 1981), p. 173.

[20](a) S. Huzinaga, Approximate Atomic Functions. I. Department of Chemistry Report, University of Alberta, Edmonton, Alberta, Canada, 1971; (b) F. B. van Duijneveldt, IBM Technical Research Report RJ945, No. 16437, 1971.

[21]H. J. Werner and W. Meyer, Mol. Phys. 31, 855 (1976).

[22]S. Huzinaga, J. Chem. Phys. 52, 1293 (1965).

[23]M. Dupuis, J. Rys, and H. F. King, J. Chem. Phys. 65, 111 (1976); an earlier version of this program is available: H. King, M. Dupuis, and J. Rys, National Resource for Computation in Chemistry Software Catalog, Program QHO2.

[24]D. B. Neumann and J. W. Moskowitz, J. Chem. Phys. 49, 2056 (1968); this program is available as part of the POLYATOM (version II) package: D. B. Neumann, H. Basch, R. L. Kornegay, L. C. Snyder, J. W. Moskowitz, C. Hornback, and S. P. Liebman, Quantum Chemistry Program Exchange Catalog, Program No. 199.

[25]D. G. Truhlar, D. A. Dixon, and R. A. Eades, J. Phys. B 12, 1913 (1979).

[26]J. C. Slater and J. G. Kirkwood, Phys. Rev. 37, 682 (1931).

[27]E. A. Mason and L. Monchick, Adv. Chem. Phys. 12, 329 (1967).

[28]G. F. Thomas and W. J. Meath, Mol. Phys. 34, 113 (1977).

[29]R. W. Kiser, *Introduction to Mass Spectroscopy and Its Applications* (Prentice–Hall, Englewood Cliffs, New Jersey, 1965), p. 314.

[30]J. L. Walsh, J. H. Ahlberg, and E. N. Nilson, J. Math. Mech. 11, 225 (1962).

[31]D. G. Truhlar, N. M. Harvey, K. Onda, and M. A. Brandt, in *Algorithms and Computer Codes for Atomic and Molecular Scattering Theory*, edited by L. D. Thomas (Lawrence Berkeley Laboratory, Berkeley, California, 1979), Vol. I, p. 220; M. A. Brandt, D. G. Truhlar, K. Onda, and D. Thirumalai, NRCC Software Catalog (Lawrence Berkeley Laboratory, Berkeley, California, 1980), program No. KQ12. NRCC codes are now distributed by the National Energy Software Center, Argonne National Laboratory, Argonne, Illinois, and by the Quantum Chemistry Program Exchange, Department of Chemistry, Indiana University, Bloomington, Indiana.

[32]G. A. Parker, B. R. Johnson, and J. C. Light, in *Algorithms and Computer Codes for Atomic and Molecular Scattering Theory*, edited by L. D. Thomas (Lawrence Berkeley Laboratory, Berkeley, California, 1980), Vol. II, p. 101; G. A. Parker, J. C. Light, and B. R. Johnson, Chem. Phys. Lett. 73, 572 (1980).

[33]L. D. Thomas, M. H. Alexander, B. R. Johnson, W. A. Lester, Jr., J. C. Light, K. D. McLenithan, G. A. Parker, M. J. Redmon, T. G. Schmalz, D. Secrest, and R. B. Walker, J. Comput. Phys. 41, 407 (1981).

[34]G. A. Parker, J. V. Lill, and J. C. Light, NRCC Softwave Catalog (Lawrence Berkeley Laboratory, Berkeley, California, 1980), Program KQ04. See Ref. 31 for availability.

[35]B. R. Johnson, J. Comput. Phys. 13, 445 (1973).

[36]C. A. Parker, T. G. Schmalz, and J. C. Light, J. Chem. Phys. 73, 1757 (1980).

[37]K. Onda and D. G. Truhlar, J. Chem. Phys. 69, 1361 (1978). This test case was later [K. Onda and D. G. Truhlar, J. Chem. Phys. 70, 1681 (1979)] labeled potential i for e^--N_2 scattering.

[38]K. Onda and D. G. Truhlar, J. Chem. Phys. 71, 5097 (1979).

[39]L. J. Kieffer, At. Data 2, 293 (1971).

[40]E. Barbarito, M. Basta, M. Calicchio, and G. Tessari, J. Chem. Phys. 71, 54 (1979).

[41]R. A. Buckingham, H. S. W. Massey, and S. R. Tibbs, Proc. R. Soc. London Ser. A 178, 119 (1941).

[42]J. Callaway, Comput. Phys. Commun. 6, 265 (1974).